Nano Energy 103 (2022) 107807

Contents lists available at ScienceDirect

Nano Energy

journal homepage: www.elsevier.com/locate/nanoen

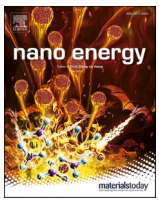

Fully stretchable, porous MXene-graphene foam nanocomposites for energy harvesting and self-powered sensing

Li Yang [a,*], Chaosai Liu [c], Wenjing Yuan [b], Chuizhou Meng [c], Ankan Dutta [d], Xue Chen [e], Langang Guo [c], Guangyu Niu [f], Huanyu Cheng [d,*]

[a] State Key Laboratory of Reliability and Intelligence of Electrical Equipment, School of Health Sciences and Biomedical Engineering, Hebei University of Technology, Tianjin 300130, China
[b] Tianjin Key Laboratory of Materials Laminating Fabrication and Interface Control Technology, School of Materials Science & Engineering, Hebei University of Technology, Tianjin 300130, China
[c] State Key Laboratory for Reliability and Intelligence of Electrical Equipment, Hebei Key Laboratory of Smart Sensing and Human-Robot Interaction, School of Mechanical Engineering, Hebei University of Technology, Tianjin 300401, China
[d] Department of Engineering Science and Mechanics, The Pennsylvania State University, University Park 16802, USA
[e] State Key Laboratory of Reliability and Intelligence of Electrical Equipment, Key Laboratory of Bioelectromagnetics and Neuroengineering of Hebei Province, School of Electrical Engineering, Hebei University of Technology, Tianjin 300130, China
[f] School of Architecture and Art, Hebei University of Technology, Tianjin 300130, China

ARTICLE INFO

Keywords:
Triboelectric nanogenerator (TENG)
MXene-graphene foam nanocomposites
Ag NWs/LIG composites
Fully stretchable
Energy harvesting and self-powered sensing

ABSTRACT

The growing demand for intelligent wearable electronic devices has spurred the rapid developments of high-performance deformable power supplies such as triboelectric nanogenerators (TENGs) with high output performance. However, the intrinsically stretchable TENGs especially those prepared with low-cost manufacturing approaches still suffer from poor performance. To address the challenge, this paper presents a fully stretchable TENG consisting of an intrinsically stretchable MXene/silicone elastomer and silver nanowires (Ag NWs)-graphene foam nanocomposite. The intrinsically stretchable TENG exhibits high output performance (voltage, current, and power of 73.6 V, 7.75 μA, and 2.76 W m^{-2}), long-term reliability, and stable electrical output under various extreme deformation conditions. In addition to the application on the human skin and clothing for human motion monitoring and detecting the strength training postures, the intrinsically stretchable TENG can also harvest the intermittent mechanical energy from human bodies to charge various energy storage units such as commercial capacitors for driving wearable electronic devices. The resulting systems have been demonstrated in applications from home anti-theft to water resources early warning systems, which provide the proof-of-the-concept demonstrations for the next-generation standalone device platforms.

1. Introduction

The rapid development of wearable electronics in the past few decades has created new demand for a consistent and reliable power supply. The commonly used rigid, bulky batteries that need to be recharged or replaced [1–5] often limit the applicability and service life of wearable electronics. As a promising alternative, triboelectric nanogenerators (TENGs) have recently received much attention to harvest low-frequency mechanical energy into electric energy based on triboelectrification and electrostatic induction, which can provide a flexible power supply and self-powered sensing systems. Compared to the flexible TENG operating in vertical contact-separation [6–9], lateral sliding [10–13], and freestanding triboelectric-layer modes [18–21], single-electrode TENGs [14–17] with suitable output performance and wearability are more promising in skin-mounted electronics due to their simple structure and portability [22,23]. Different from metal [24–27] and conductive polymer [28,29], graphene [30–33] exhibits outstanding electrical properties and high flexibility [34–36] for use as electrodes. However, the complicated synthesis and small flake size of graphene have largely limited the application of the graphene-based TENG. Owing to the low cost and high conductive nature, laser-induced graphene (LIG) foams have been explored as electrodes in TENG [37–41], but LIG electrodes are susceptible to cracking at less than 5% strain due to their insufficient energy dissipation [42,43]. The

* Corresponding authors.
E-mail addresses: yangli5781@126.com (L. Yang), huanyu.cheng@psu.edu (H. Cheng).

https://doi.org/10.1016/j.nanoen.2022.107807
Received 13 July 2022; Received in revised form 27 August 2022; Accepted 13 September 2022
Available online 15 September 2022

LIG-based TENG with good stretchability and high output performance is yet to be demonstrated for wearable, long-term applications.

MXene with outstanding conductivity (>20,000 S cm^{-1}) [44,45] contains abundant surficial –F groups, making it triboelectrically more negative than commonly used polytetrafluorethylene. Although MXene has been explored as the electrode material in TENG [65–67], it is associated with low conductivity, high cost, and compromised performance. Meanwhile, the direct use of MXene as a triboelectric material is often combined with non-stretchable electrode to result in non-stretchable TENG [27,68], although the output performance is relatively good. Herein, this work combines the stretchable Ag nanowires (NWs)/LIG electrodes prepared by the pre-strain strategy with the porous MXene/polydimethylsiloxane (PDMS)-Ecoflex film to create an intrinsically stretchable TENG operating in the single-electrode mode. The pre-strained Ag NWs/LIG electrode (pre-strain level of 30%) exhibits excellent conductivity (~62.5 S/cm), simple manufacturing at low cost, large specific surface area (~340 m^2/g) [46], and improved triboelectric performance in the output voltage, current density, and charge density. The use of PDMS-Ecoflex composite in both the triboelectric and substrate layers also provides lower modulus, larger stretchability, and higher compliance, while allowing successful integration of MXene and LIG. Moreover, the insolubility of MXene aqueous solution in the PDMS-Ecoflex elastomer facilitates the formation of a porous structure, which enhances the triboelectronegativity, the surface contact area, and surface charge density. The resulting TENG based on porous MXene-LIG foam exhibits an open circuit voltage of 73.6 V, a

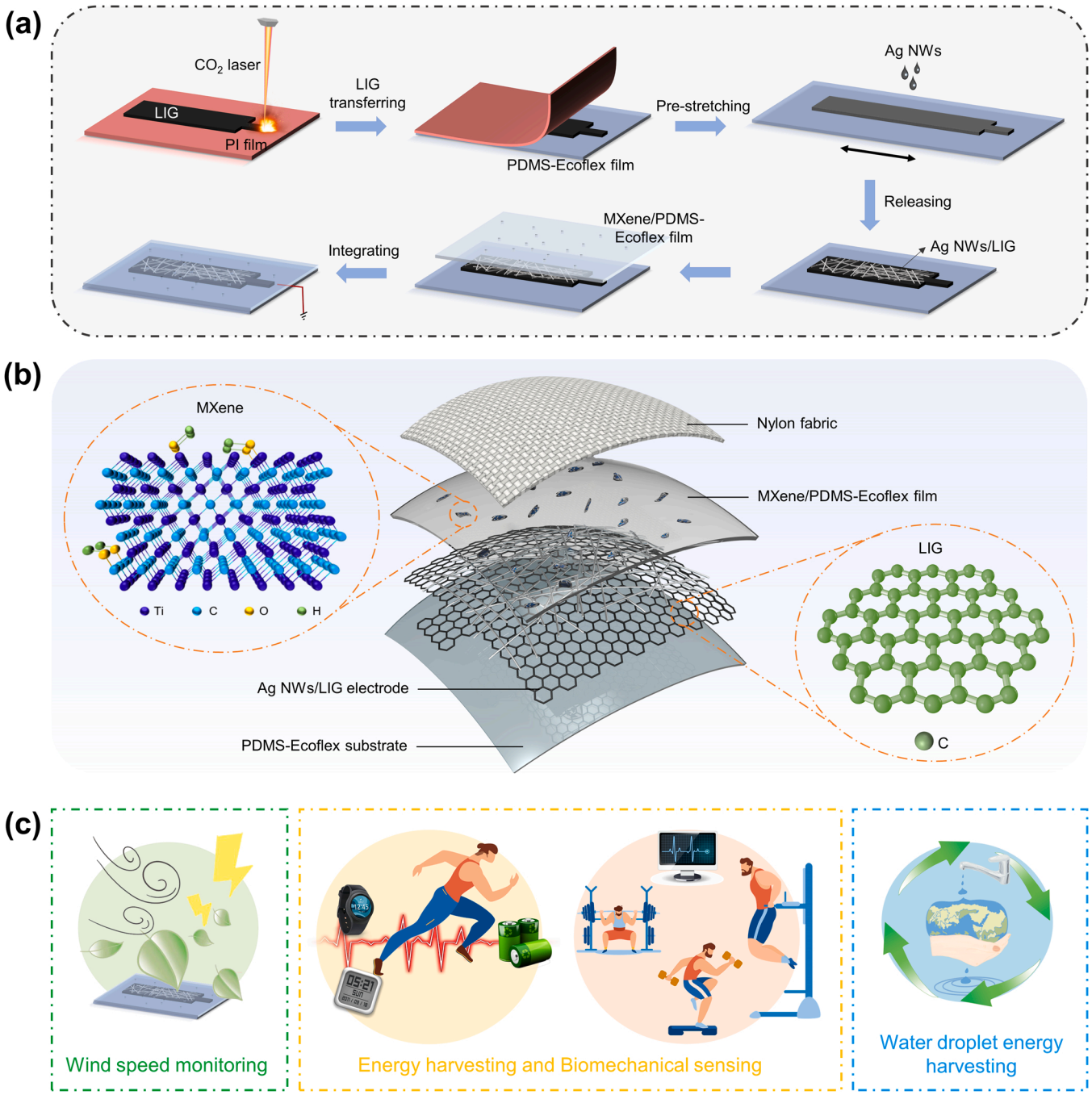

Fig. 1. Schematic diagrams showing the (a) preparation, (b) structure, and (c) application of the stretchable porous MXene/LIG foam-based TENG in human motion energy harvesting, biomechanical sensing, wind speed monitoring, and water droplet energy harvesting.

short circuit current of 7.75 μA, and durable performance under 30% stretching. Besides attachment onto various substrates (clothes, skin, and leaf surface) to detect human activities and wind speeds, the stretchable porous MXene-LIG-based TENG can also harvest mechanical energy to power low-power electronic devices. The proof-of-concept demonstrations on exercise posture detection, home anti-theft, and water resources early warning systems highlight the potential applications and development prospects in soft robots, green energy, human-computer interaction, and wearable electronic products.

2. Results and discussion

2.1. Fabrication of the stretchable TENG based on MXene-LIG foams

The preparation of the stretchable TENG based on the MXene/LIG foam (Fig. 1a) starts with the fabrication of 3D porous LIG foam electrodes (2 ×2 cm^2) by direct laser heating of the 75 μm-thick PI film (Fig. S1a). Next, curing the mixed solution of the PDMS and Ecoflex with a mass ratio of 1:1 on the LIG/PI surface for 2 h is followed by peeling to transfer the LIG electrodes to the flexible silicon rubber substrate. Compared to PDMS, the PDMS-Ecoflex film exhibits improved flexibility and stretchability [47] with the strain at fracture increased by ca. 145% (Fig. S2). Although pure Ecoflex is more stretchable than PDMS-Ecoflex, it cannot completely transfer LIG from the PI film, leading to the choice of PDMS-Ecoflex. After applying pre-strain and spray coating the Ag NWs solution on pre-stretched LIG/PDMS-Ecoflex electrodes, the release of the pre-strain prepares the stretchable Ag NWs/LIG electrodes. The preparation of MXene/PDMS-Ecoflex composite film relies on spin coating and curing of the MXene in PDMS-Ecoflex solution on the glass substrate (Fig. S3), where the MXene ($Ti_3C_2T_x$) nanosheet solution is synthesized by selectively etching the aluminum layer from Ti_3AlC_2. The integration of the porous MXene/PDMS-Ecoflex film with the Ag NWs/LIG electrode yields a highly stretchable TENG (Figs. 1b and S1). The contact of the stretchable TENG based on porous MXene/graphene foam with the Nylon fabric provides application opportunities in energy harvesting, self-powered sensing, and standalone stretchable device platforms. The representative proof-of-the-concept demonstrations include exercise posture detection, home anti-theft, water resources early warning, water droplets energy harvesting, human motion, and wind speed monitoring systems (Fig. 1c).

2.2. Material characterization of the stretchable porous MXene-based TENG

The highly porous 3D graphene networks formed from the release of gaseous products facilitate the infiltration of the PDMS-Ecoflex prepolymer for successful transfer of the LIG (Figs. 2a and S5a). The Raman spectra of the LIG/PDMS-Ecoflex (Fig. S5b) exhibit distinct

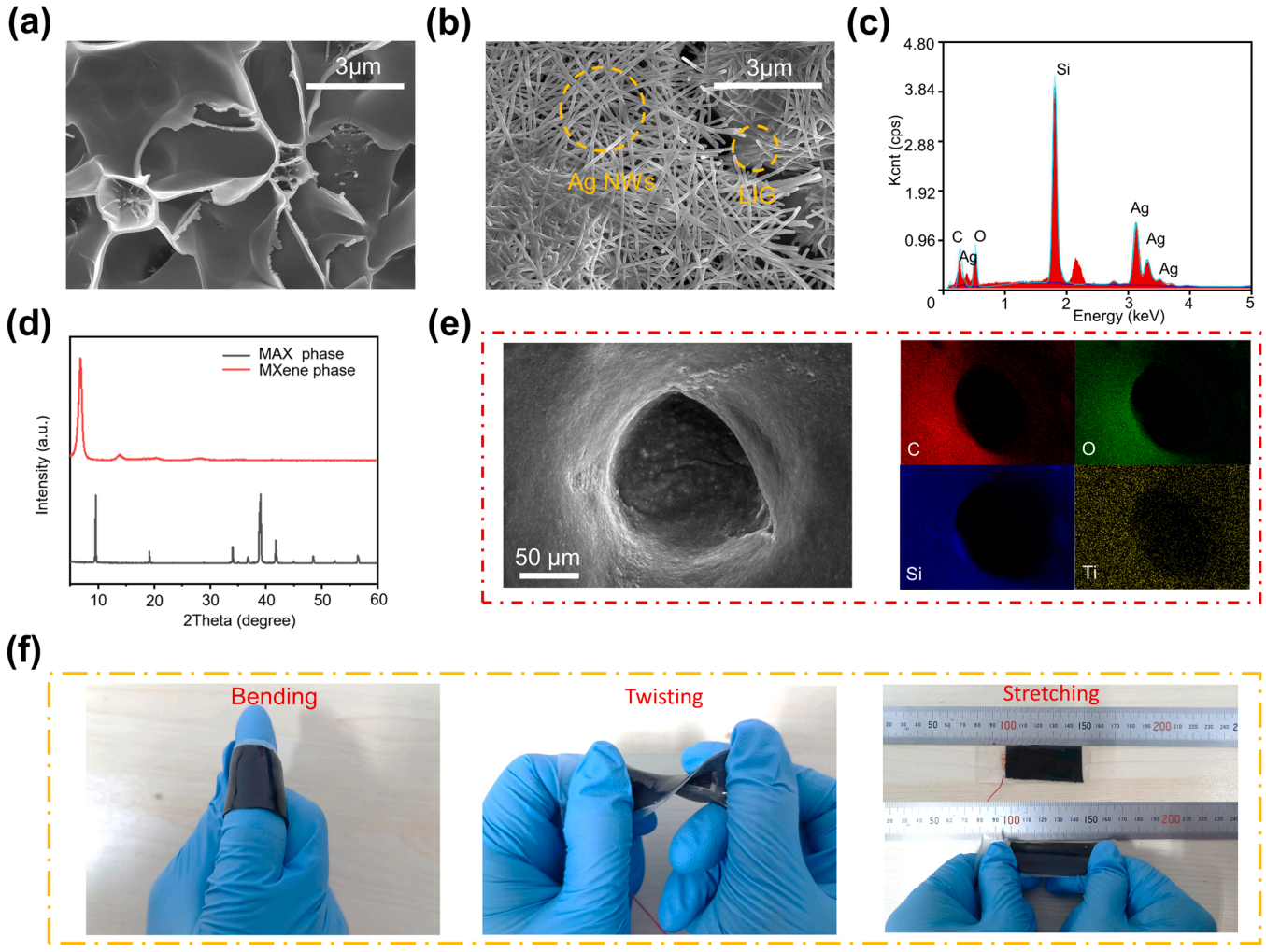

Fig. 2. Characterizations of the stretchable porous MXene/PDMS-Ecoflex TENG. SEM images of the transferred porous LIG (a) before and (b) after coating of the Ag NWs. (c) Energy Dispersive Spectroscopy (EDS) spectrum of Ag-coated LIG/PDMS-Ecoflex electrode. (d) XRD patterns of bulk MAX phase (Ti_3AlC_2) and MXene ($Ti_3C_2T_x$). (e) Elemental mapping analysis of MXene/PDMS-Ecoflex composite film for C, O, Si, and Ti. (f) Optical images of the MXene/PDMS-Ecoflex under bending, twisting, and stretching.

characteristic D (~1350 cm^{-1}), G (~1572 cm^{-1}), and 2D peaks (~2697 cm^{-1}), with a reasonably large value of the I_{2D}/I_G ratio, to confirm the presence of few-layered porous graphene [50]. The uniform distribution of Ag NWs on the 3D porous LIG/PDMS-Ecoflex (Figs. 2bc and S5c) allows a sharp reduction of the sheet resistance from 48.6 to 4.2 Ω/□ even without pre-stretching, as measured by a four-point probe instrument (Fig. S4). With a pre-strain of 30%, the sheet resistance of the Ag NWs/LIG electrode is further decreased to 3.2 Ω/□, due to higher Ag NWs loading from the pre-strained area [51].

The MXene ($Ti_3C_2T_x$) nanosheets with the accordion-like structure [48,49] (Fig. S6) are confirmed by the broadened (002) peak that is decreased from 9.5° to 6.6° in the X-ray diffraction (XRD) after etching Ti_3AlC_2 (MAX) (Fig. 2d). The MXene nanosheets in PDMS-Ecoflex also provide the composite film with randomly distributed mesoporous structures (Fig. S7ab). The MXene nanosheets are uniformed the distributed in the PDMS-Ecoflex around the pores, as evidenced by the characteristic elements Ti and Si of MXene and silicon rubber in the energy dispersive spectrometer mapping, respectively (Fig. 2e). The porous MXene/PDMS-Ecoflex composite is also highly flexible and stretchable to undergo various mechanical deformations such as bending, twisting, and stretching (Fig. 2f).

2.3. *Working mechanism and output performance of the stretchable TENG*

The operation of the stretchable MXene-based TENG relies on the coupled triboelectrification and electrostatic induction between the MXene/PDMS-Ecoflex (frictional negative layer) and a nylon fabric (movable frictional positive layer) as an electron donor (Fig. 3ab). With the stretchable TENG connected to the ground through wires in single-electrode mode, the initial full contact between the nylon fabric with the MXene/PDMS-Ecoflex induces the charge transfer from nylon to the composite on the contact surface due to contact electrification. The positively charged nylon fabric surface and the negatively charged MXene/PDMS-Ecoflex surface can maintain a static equilibrium state due to negligible dipole moments (Fig. 3ab-i). After the nylon fabric is moved away from the MXene/PDMS-Ecoflex, the separation of opposite charges forms strong dipole moments to generate a potential difference between the composite and the ground (Figure 3ab-ii). The unshielded negative charges on the MXene/PDMS-Ecoflex surface cause electrostatic induction of the electrode to create transient charges flow from the electrode to the ground and generate voltage outputs. Electrostatic equilibrium is achieved when the distance between the oppositely charged MXene/PDMS-Ecoflex and nylon fabric reaches a maximum (Fig. 3ab-iii). When the nylon fabric approaches the MXene/PDMS-Ecoflex till full contact, the previous electrostatic equilibrium is disturbed and the potential difference decreases, causing the charge to flow back to the electrode from the ground for generating an opposite electrical signal (Fig. 3ab-iv). Therefore, the repeated contact-separation cycles generate alternating voltage and current to convert mechanical energy into electrical energy. Among 25 different commercial fabric samples with the voltage scatter diagram shown in Fig. S8, the stretchable TENG with the nylon fabric exhibits the best output performance, as Nylon is from the top of the triboelectric series [52]. Compared with the five typical fabrics (Fig. 3c and S9ab), the stretchable TENG with the nylon fabric and triboelectronegative PDMS-Ecoflex gives an open-circuit voltage of 20 V, short-circuit current density of 5.3 mA/m^2, and charger transfer density of 34.8 μC/m^2 for an applied force of 15 N at a frequency of 5 Hz. Compared with the other triboelectronegative materials (e.g., pure PDMS or PDMS-Ecoflex), the stretchable TENG based on MXene/PDMS-Ecoflex produces the highest output performance with the open-circuit voltage of 40 V, short-circuit current density of 10.6 mA/m^2, and charger transfer density of 69.1 μC/m^2 (Fig. 3d and S9cd). The significantly enhanced voltage and current result from the high electrical conductivity of MXene (for enhanced charge transfer) and increased electronegativity (due to the introduced –F and terminated oxygen-containing functional groups) from MXene nanosheets. In addition, the output performance of TENG depends on the MXene concentration (Fig. S10). The output performance of TENG first increases with the increased concentration of MXene (1–5 mg/ml), which is due to

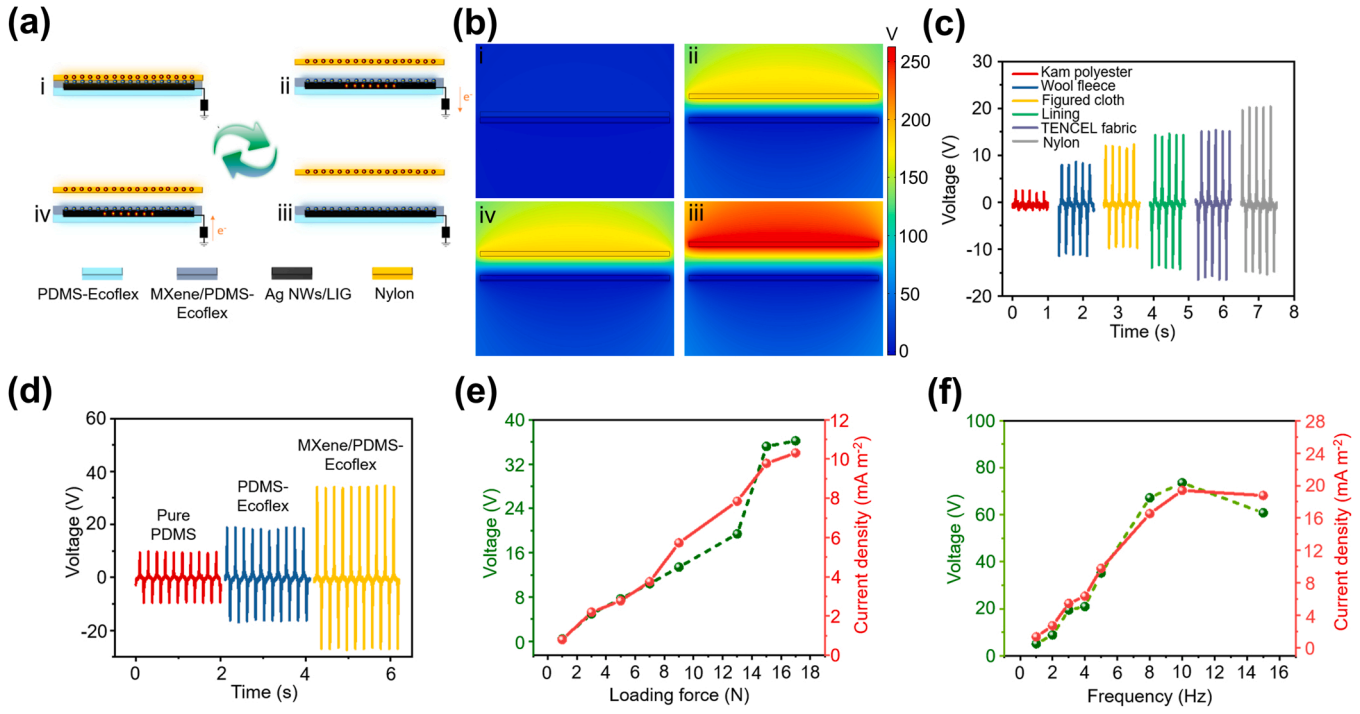

Fig. 3. Working mechanism and output performance of the stretchable porous MXene-based TENG. (a) Schematic diagram and (b) finite element simulation results to show the charging distribution. Comparison of the output voltage of the TENG with various (c) types of fabrics and (d) triboelectric layers. Output voltage and current of the TENG as a function of (e) applied force and (f) contact-separation frequency. The dimension of the TENG is fixed as 2.0 × 2.0 cm^2 in this set of measurements.

the enhanced electronegativity and electrical conductivity from a higher concentration of MXene. However, the further increase in the concentration from 5 to 7 mg/ml results in slightly decreased output performance, which is likely attributed to the aggregation of MXene [38]. Therefore, the added concentration of MXene is optimized to be 5 mg/ml in the following experiments. Although the MXene/PDMS-Ecoflex film can be combined with a more conductive electrode such as Cu (Fig. S11), the output performance actually becomes lower than that combined with the Ag NWs/LIG electrode (Fig. S12), indicating the synergistic effect between the two. In particular, the MXene/PDMS-Ecoflex film with the Ag NWs/LIG electrode exhibits an increase of 74.5%, 61.9%, and 59.6% in the open-circuit voltage, short-circuit current density, and charge density compared to that with Cu, confirming the synergistic effect between the two. Compared with the TENG with Ag NWs electrode, the one with LIG exhibits higher output performance due to a large specific surface area, whereas further enhancement is observed in the one with the Ag NWs/LIG electrode (Fig. S13). In particular, the Ag NWs/LIG-based TENG demonstrates 307.4%, 181.3%, and 87.2% higher in open-circuit voltage, short-circuit current density, and charge density than that without LIG. At a fixed frequency of 5 Hz, both the open-circuit voltage and short-circuit current density gradually increase as the applied force increases from 1 to 15 N, but their values are almost saturated when the force reaches 17 N (Figs. 3e and S14ab). The changes may be attributed to the increase and saturation of the effective static frictional contact [41] between the inner and surface structure of the MXene/PDMS-Ecoflex as the applied force increases from 1 to 15 and then to 17 N. For a loading force of 15 N, the open-circuit voltage and short-circuit current of the TENG gradually increase to the maximum output voltage of 73.6 V and current density of 19.4 mA/m^2 as the frequency increases from 1 to 10 Hz, due to the surface charge accumulation (Figs. 3f and S14cd). As the frequency increases, the rate of charge accumulation on the surface of TENG increases, facilitating the charge transfer to the corresponding external circuit. As a result, the short-circuit current as the derivative of charge to time also increases [41,55,61]. However, the further increase in the frequency from 10 to

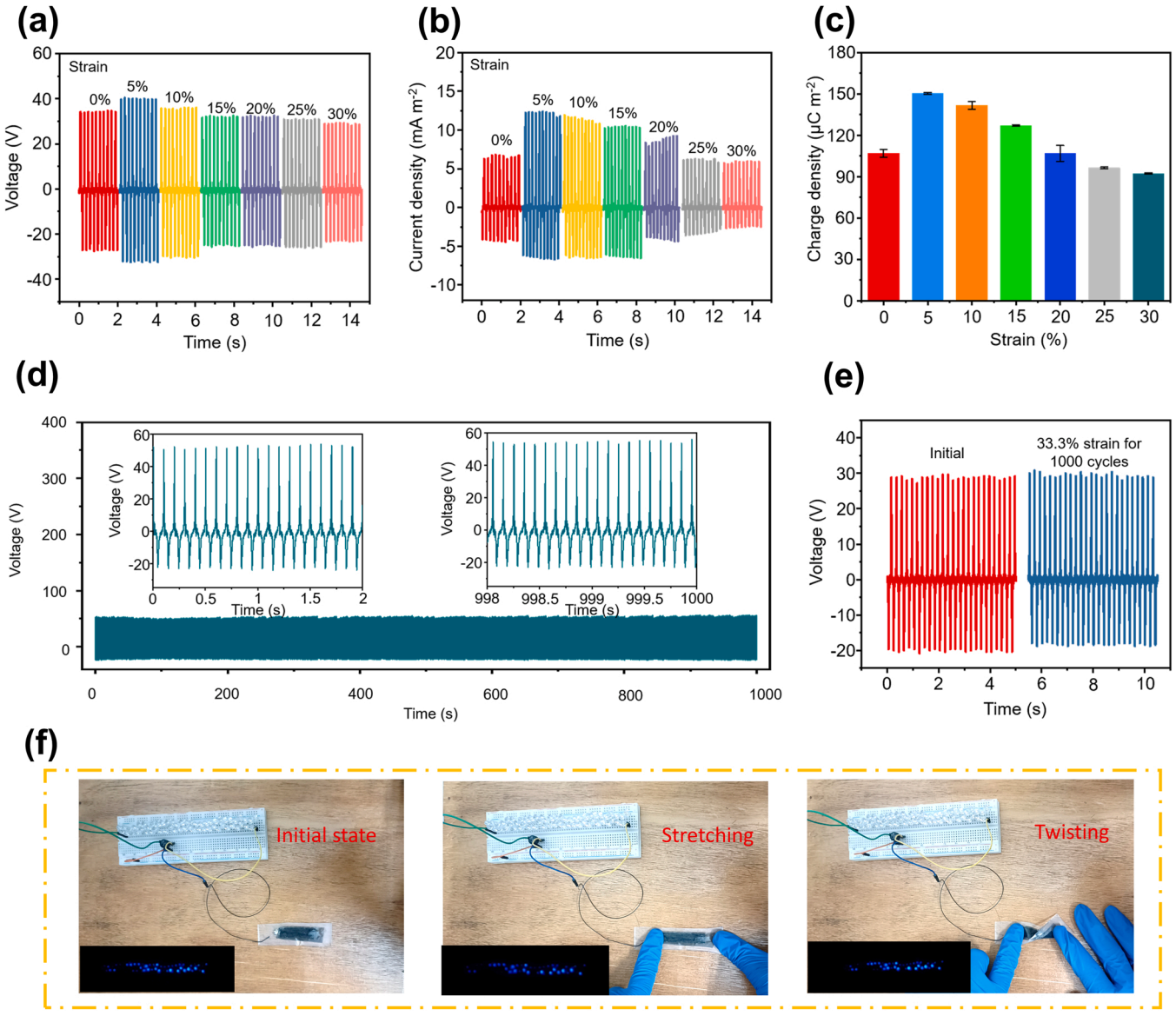

Fig. 4. Deformability and durability of the stretchable porous MXene-based TENG. (a) Output voltage, (b) current density, and (c) charge density of the stretchable TENG at various stretching levels (for a vertical driving force of 15 N at a frequency of 5 Hz). (d) The durability test of the TENG over 10,000 cycles, with partially enlarged views shown in the inset (for a vertical driving force of 10 N at a frequency of 10 Hz). (e) Comparison of the output voltage of the TENG before and after 30% tensile strain for 1000 cycles. (f) Photograph of 57 LEDs lit by the TENG in initial, stretching, and twisting states.

15 Hz results in slightly decreased output performance, which is likely attributed to charge loss caused by air breakdown at high operating frequency [27,39,62]. As the increased voltage generated in the air gap from the increased charge density reaches the breakdown voltage [63,64], the dissipated electrostatic energy due to the air breakdown lowers the TENG output. Therefore, the optimal operation conditions with the applied force of 15 N at a frequency of 10 Hz are used in the following studies unless otherwise specified.

2.4. Deformability and durability of the stretchable porous MXene-based TENG

Deformability and durability of the stretchability TENG come from the stretchable Ag NWs/LIG electrode integrated with the MXene/PDMS-Ecoflex. Compared with the LIG electrode that shows a resistance change of 840% upon the tensile strain of 30%, the Ag NWs/LIG electrode exhibits a much lower resistance of 30% (Fig. S15a). With the use of the pre-strain strategy on LIG before spraying Ag NWs solution, the stretchability of Ag NWs/LIG electrodes is further enhanced to give an even smaller resistance change (e.g., 23% upon 30% stretching for the electrode created from a pre-strain of 30%) (Figs. S15b and S16). The change in resistance of the Ag NWs/LIG electrode from a pre-strain of 30% is only 2% for a cyclic loading/unloading strain of 10% over 1000 cycles (Fig. S15c). The output performance of the stretchable porous MXene-based TENG reaches the maximum with the voltage of 40.4 V, current density of 12.4 mA/m^2, and charge density of 150 μC/m^2 at a tensile strain of 5% (Fig. 4a-c). However, the output performance gradually decreases as the tensile strain further increases from 5% to 30%. This result is likely attributed to the initially increased and then decreased effective contact surface area of the Ag NWs/LIG electrode upon stretching [53]. In addition, the stability of the stretchable MXene-based TENG is measured by long-term cyclic testing, The stretchable TENG also exhibits stable output performance over 10,000 cycles (for 10 N driving force at 10 Hz) (Fig. 4d) or cyclic stretching of 33.3% over 1000 cycles (Fig. 4e). The stable and durable performance of the stretchable TENG allows it to drive 57 LEDs even upon stretching and twisting (Fig. 4f and Video S1).

Supplementary material related to this article can be found online at

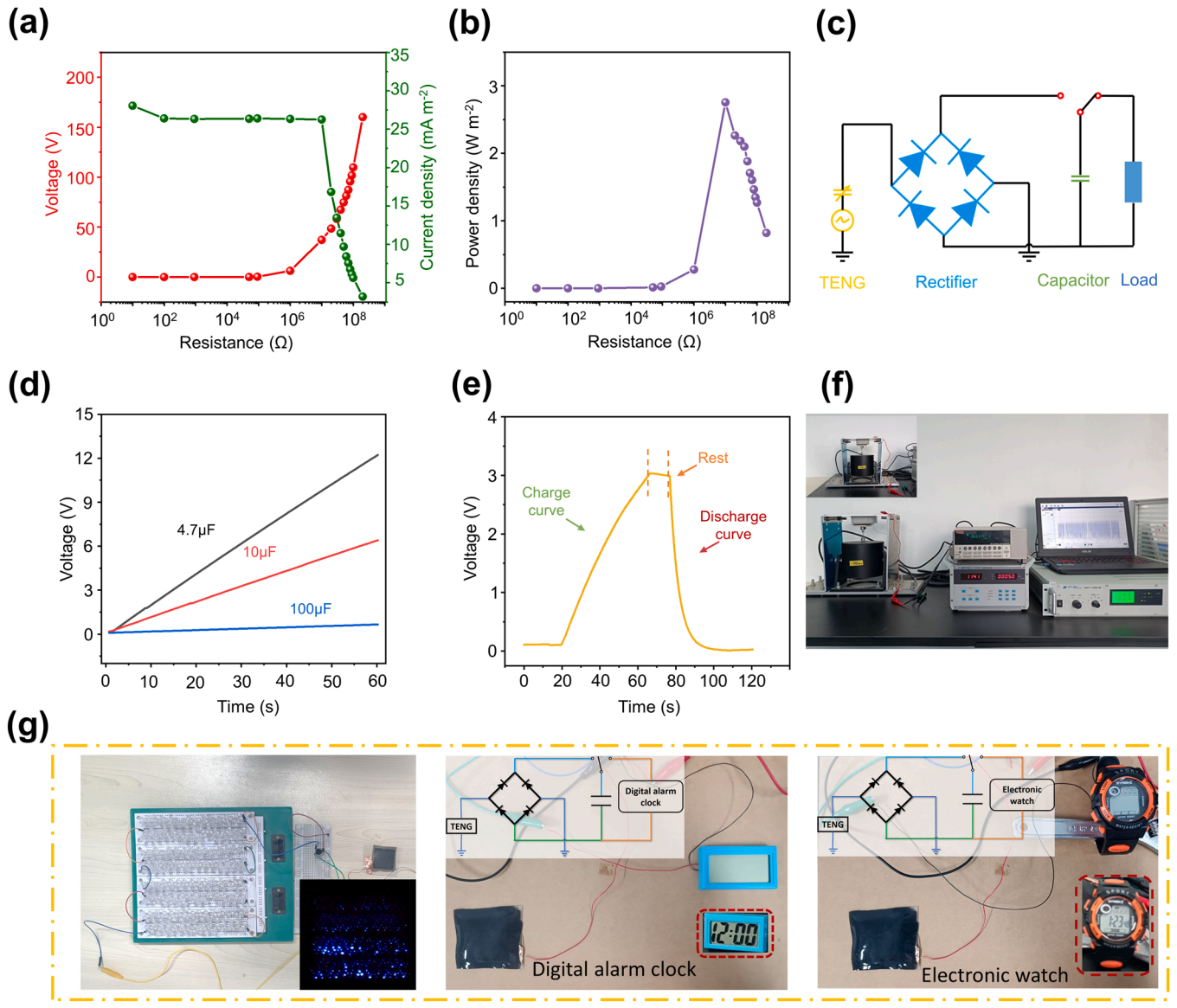

Fig. 5. Mechanical energy harvesting performance of the stretchable MXene-based TENG. (a) Output voltage, current, and (b) power density of the stretchable TENG as a function of the external load resistance. (c) Circuit model of the self-charging TENG-based system. (d) Charging curves of the three commercial capacitors by the stretchable TENG. (e) Charging and discharging curves of the capacitor by the TENG with a power management unit. (f) Optical image to show the setup of the mechanical energy harvesting system, and its demonstrations to drive (g) 391 LEDs, a low-power electronic clock, and an electronic watch.

doi:10.1016/j.nanoen.2022.107807.

2.5. Mechanical energy harvesting by the stretchable porous MXene-based TENG

The mechanical energy harvesting performance of the stretchable porous MXene-based TENG is first evaluated as a function of the external load resistance ranging from 10 to 200 MΩ (Fig. 5ab). The output voltage (current) increases (decreases) with the increasing external load resistance (Fig. 5a), leading to an initially increased and then decreased power density with a maximum instantaneous power density of 2.76 W m^{-2} at 10 MΩ (Fig. 5b)[54]. The stretchable TENG presented in this work with high output performance and excellent tensile properties compares favorably with the others previously reported in the literature (Tables S1 and S2). The harvested energy is often intermittent due to the nature of human motions, so exploiting the energy to charge energy storage devices such as batteries and (super) capacitors with power management circuits presents opportunities for practical applications [43,55,56]. As a proof-of-the-concept demonstration, bridge rectifiers help convert the generated alternating current from the stretchable TENG to direct current for charging the commercial capacitors before driving low-power wearable electronic devices (Fig. 5c). The charging voltage reaches 12, 6, and 0.67 V in 60 s for the capacitor of 4.7, 10, and 100 μF for a vertical driving force of 15 N at 10 Hz (Fig. 5d). The energy harvesting from repeated hand tapping at ca. 3–4 Hz also charges the 4.7 μF capacitor to 3 V in 40 s and powers an electronic watch (Fig. 5e, Fig. S17, and Video S2). The harvested energy from the exciter's vibration (Fig. 5fg) or hand tapping of 3–4 Hz can readily drive 391 LEDs (Video S3), a digital alarm clock (Video S4), and an electronic watch (Video S5), demonstrating the potential for a sustainable self-powered system.

Supplementary material related to this article can be found online at doi:10.1016/j.nanoen.2022.107807.

2.6. Human motion monitoring and posture detection by the stretchable MXene-based TENG

Although the repetition of specific postures can stimulate target muscles (e.g., the biceps, latissimus dorsi, quadriceps femoris, and pectoralis major) in strength training such as weight lifting, it is difficult to quantify and accurately monitor human posture to prevent joint injuries during exercise. To reduce the risk of severe permanent joint pain from the wrist, lower back, and knee injuries [57], the self-powered strain sensor based on the stretchable MXene-based TENG is attached to the human body to monitor posture during strength training (Fig. 6). After attaching the TENG to the skin surface (or clothes) while the joint is bent, the TENG outputs an alternating current (AC) signal due to coupled contact charging and electrostatic balance effect. Varying bending angles generate different voltage signals in the TENG due to changing effective contact areas between the MXene/PDMS-Ecoflex and skin. Two exercises (arm bending and single-arm dumbbell rowing). The device on the joint of the wrists (Fig. 6a) can effectively monitor the cyclic wrist bending as the output voltage value increases with the increasing bending angle due to the larger contact area between the device and the clothes (Fig. 6b). As a result, the high peak output voltage signal associated with a large bending angle at the wrist joint can signal the wrong posture during arm curl training (Fig. 6c). Similarly, the self-powered strain sensor attached to the lower back (Fig. 6d) can measure different back bending angles (Fig. 6e) to detect the wrong posture during one-arm dumbbell row training (Fig. 6 f). As human skin is also an excellent electron donor, the device attached to varying locations of the human body with a medical adhesive tape (Fig. S18) also

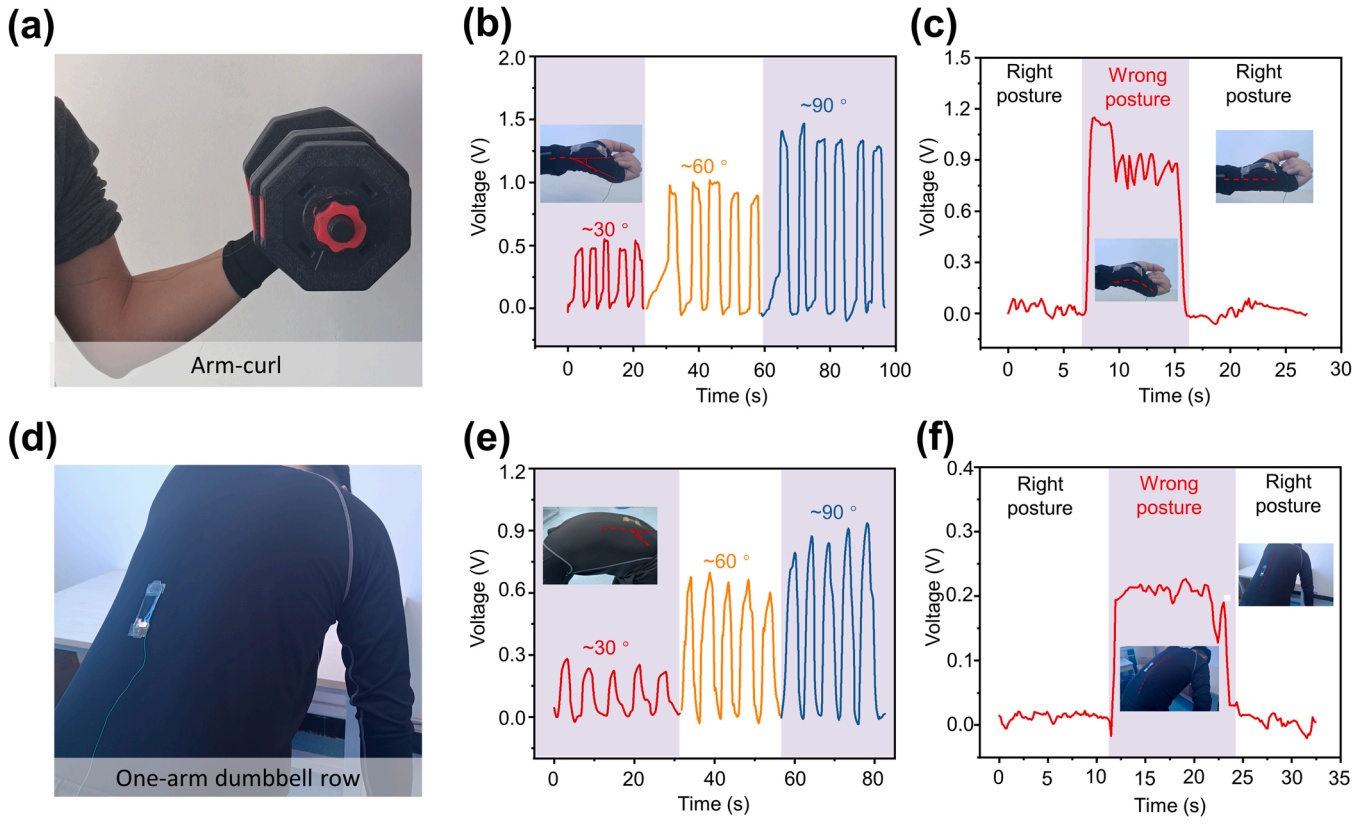

Fig. 6. Application of the stretchable MXene-based TENG for exercise posture detection. (a) Optical image of the self-power strain sensor attached to the human wrist. (b) Output from the self-power strain sensor at various wrist bending angles and (c) its demonstration to detect incorrect wrist posture in strength training. (d) Optical image of self-power strain sensor attached on human back. (e) Output from the self-power strain sensor at various back bending angles and (f) its demonstration to detect incorrect back posture.

accurately monitors the bending of the finger, elbow, and knee, breathing, and palm tapping (Fig. S19a-e), demonstrating the potential for self-powered detection of human motions.

2.7. Home anti-theft system by the stretchable MXene-based TENG

Different from a battery or AC-powered wind speed sensor, the stretchable TENG attached to the leaf surface (with primary components of cellulose and plant protein [58]) allows for self-powered wind speed monitoring as plant leaves oscillate with the wind (Fig. 7a). As the wind speed increases, the output current also increases (Figs. 7b and S20), which provides a working principle for home intrusion prevention (Figs. 7c and S21). The plants normally used for decoration and air purification can be integrated with the self-powered device and set to standby mode after the owner leaves. As a thief passes the plant, the current output from the TENG increases (Fig. 7d) and the alarm is triggered immediately, with the warning light turned on and the buzzer rang (Fig. 7e and Video S6). The sensitivity of the self-powered home anti-theft system is reasonably high, which can even be triggered by a leaf gently placed on (Video S7) or human body repeatedly passing through (Fig. S22 and Video S8).

Supplementary material related to this article can be found online at doi:10.1016/j.nanoen.2022.107807.

2.8. Early warning system by the stretchable MXene-based TENG to protect water resources

As water plays a vital role in human survival and development, it is important to optimize and save water resources. A water resources early warning system is triggered by the falling of water droplets (Fig. S23) and can convert the potential energy of water droplets into electric energy for charging the capacitor (Video S9). When the capacitor voltage reaches the preset warning value, the sound and warning light can also be turned on to alert for faucet leakage. As the voltage decreases with the increasing frequency (Fig. 8c), the much larger frequency from water flow would give a vanishing voltage value, so the water resources early

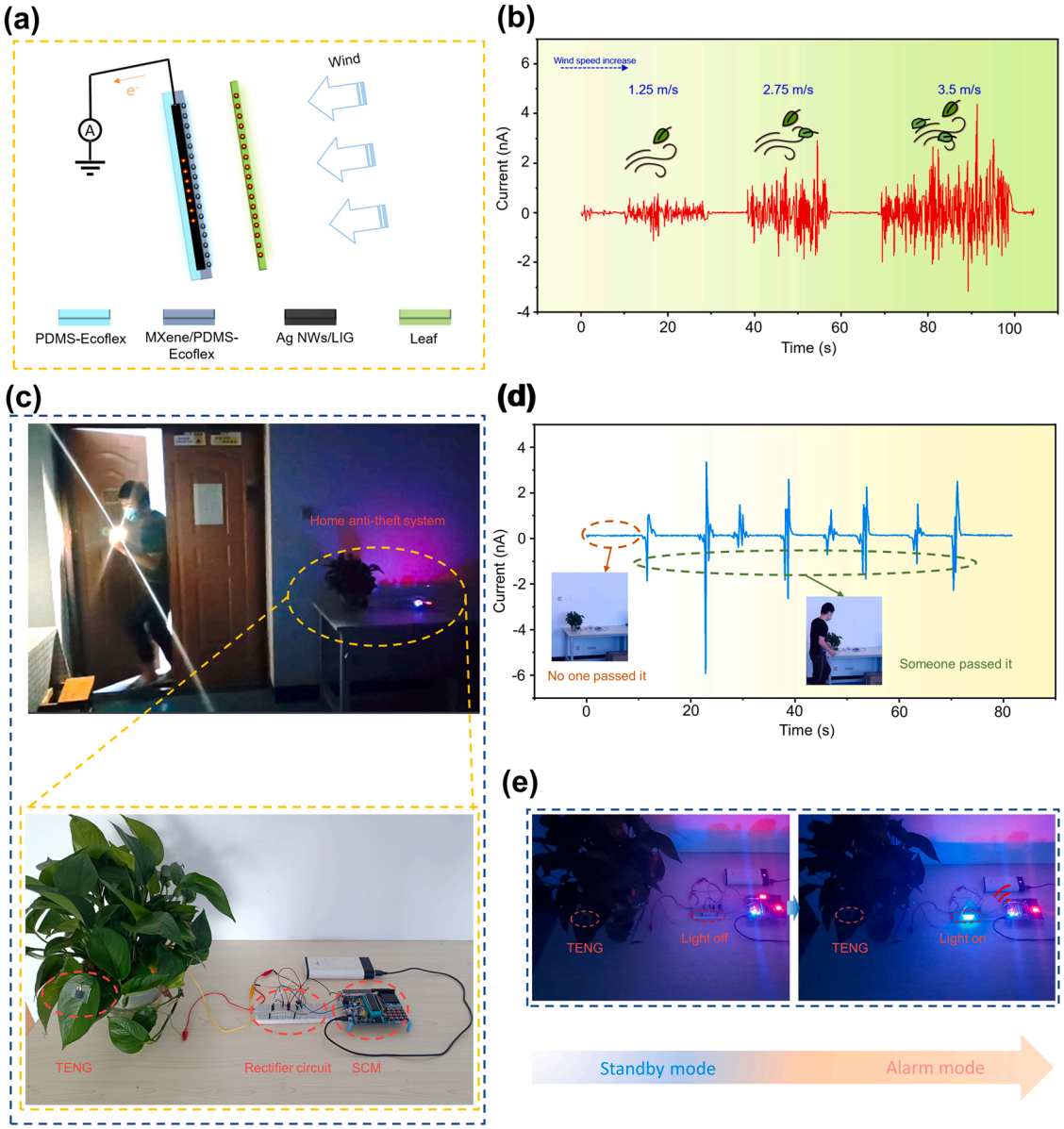

Fig. 7. Home anti-theft system based on the stretchable MXene-based TENG. (a) The working mechanism of the TENG for monitoring the wind speed and (b) its output voltage under various wind speeds. (c) Schematic diagram of the home anti-theft system and (d) its output current changes without and with a thief passing by, along with (e) the LED turning on during the simulated scene of burglar intrusion.

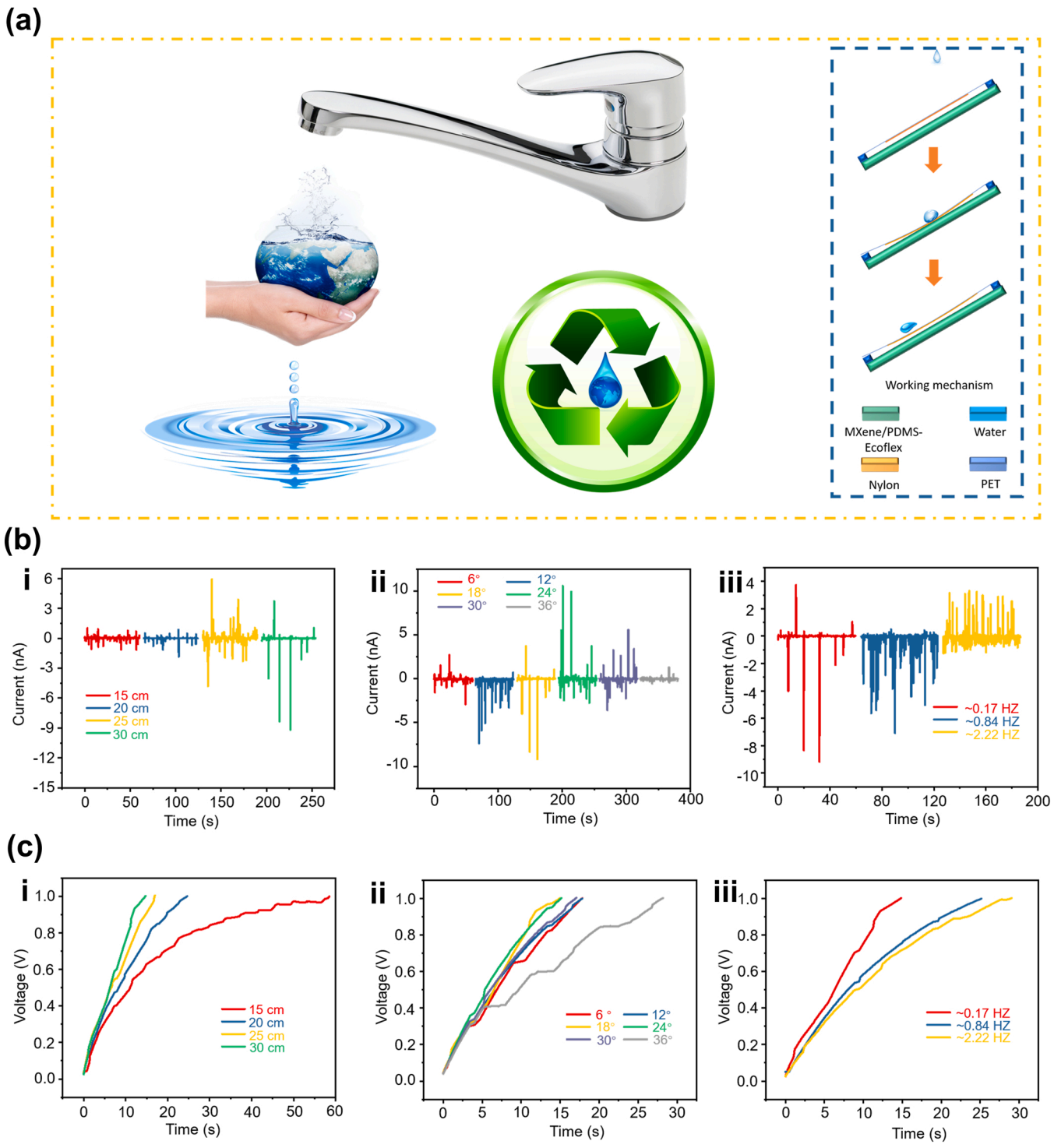

Fig. 8. Early warning system based on the stretchable MXene-based TENG for protecting water resources. (a) Operation principle of the stretchable TENG to detect falling of water droplets with (b) output current and (c) charging voltage of a capacitor of 100 nF as a function of (i) falling height, (ii) inclined angle, and (iii) dripping frequency.

warning system does not alarm during hand washing (Video S10). Different from the previously reported water-driven devices [59,60], the surface of TENG does not need to be superhydrophobic as our device is driven by the potential energy of water droplets (Fig. 8a). The nylon fabric on the 100 μm-thick polyethylene terephthalate (PET) film serves as a movable frictional positive layer, which is driven by water droplets to produce continuous AC output. As the water droplets fall and slide down the PET surface, the PET film first bends and then recovers to result in contact and separation between nylon and MXene/PDMS-Ecoflex, which generates alternating currents in the TENG from repeated droplets motion. As the driving force comes from the potential energy, the output current increases with the increasing drop height to reach a maximum mean square root of 6.5 nA at 30 cm in the range (Fig. 8b-i), which charges the capacitor of 100 nF to 1 V in 14.7 s (Fig. 8c-i). As the inclined angle increases, the output current first increases and then decreases to a mean square root current of 7.5 nA at

24° (Fig. 8b-ii), which charges the capacitor to 1 V within 15 s (Fig. 8c-ii). The effect of the inclined angle on the current likely comes from the changes in the effective bending of the PET film and the slipping conditions of water droplets on PET. The output current also gradually decreases with the increasing frequency of water dripping from 0.17 to 2.22 Hz (Fig. 8b-iii) with the capacitor charging time (to 1 V) extended from 14.7 to 29 s (Fig. 8c-iii), as the nylon and MXene/PDMS-Ecoflex cannot be effectively separated at a high frequency of water dripping.

Supplementary material related to this article can be found online at doi:10.1016/j.nanoen.2022.107807.

3. Conclusions

In summary, this work reports an intrinsically stretchable TENG based on Ag NWs/LIG electrode integrated with triboelectric MXene/PDMS-Ecoflex composite for efficient mechanical energy harvesting and self-powered biomechanical sensing. The optimized stretchable TENG (2 ×2 cm^2) operated in single-electrode mode can generate an open-circuit voltage of 73.6 V, short-circuit current of 7.75 μA, and power density of 2.76 W m^{-2}. The stretchable TENG with high and stable output performance under 30% tensile outperforms most of the previously reported works. The harvested energy from the stretchable TENG can efficiently charge energy storage devices such as (super)capacitors to power a variety of low-power electronic devices. Compared with many other TENGs previously reported in the literature, our intrinsically stretchable TENG with low modulus and high output performance allows it to conform to the 3D, dynamically changing surfaces such as human skin and growing leaves. As a proof-of-concept demonstration, the self-powered strain sensor with a modulus close to that of the human skin can conform to the skin to monitor human body movements for strength training posture detection, with minimal discomfort. Meanwhile, our intrinsically stretchable TENG on the leaf surface could grow with the plant leaves over months or even years for the anti-theft application, which is challenging for the rigid or flexible TENG. Therefore, the demonstrated applications of the stretchable TENG as a self-powered biomechanical sensor, home anti-theft system, and water resources early warning system open opportunities in the next-generation standalone stretchable device systems.

4. Experimental section

4.1. Materials

The polyimide (PI) film (PI, 75 μm thickness), blue LED lamps (rated working voltage of 3 V), and the fabric samples were purchased from the e-shop. The Ecoflex (EcoflexTM 00–50) and the polydimethylsiloxane (PDMS, Sylgard 184) were obtained from Smooth-on, Inc. and Dow Corning, respectively. Silver nanowires (5 mg/ml) were purchased from XFNANO Material Technology Co., Ltd. (Nanjing, China).

4.2. Synthesis of MXene ($Ti_3C_2T_x$)

MXene solution was prepared by selectively etching the Al layer from Ti_3AlC_2 via MILD etching [48,49]. In brief, 0.8 g LiF was first dissolved in 10 ml of 9 M hydrochloric acid (HCl, 35%) solution for 5 min with continuous stirring. Next, 0.5 g of Ti_3AlC_2 powder was slowly added to the solution and stirred at 1000 rpm at 35 °C for 24 h. The mixture was centrifuged (3500 rpm for 5 min each cycle) and washed with deionized (DI) water until the pH reached ca. 7. Separating the black slurry from the gray solid (non-etched Ti_3AlC_2) via vacuum filtration on a porous PTFE membrane obtained $Ti_3C_2T_x$ powder. Adding 0.5 g of the obtained powder to 100 ml of the DI water was followed by sonicating at 200 W for several min and centrifuging at 3000 rpm for 20 min (for removing suspended aggregates) to yield a 5 mg/ml MXene dispersion.

4.3. Preparation of PDMS-Ecoflex solution

The PDMS and Ecoflex solutions were first prepared at 10:1 (ratio of polymeric base to curing agent) and 1:1 (ratio of A to B solution) by magnetically stirring them at a speed of 2000 r/min for 2 min. Next, the PDMS solution was mixed with Ecoflex solution at a volume ratio of 1:1 with the same stirring conditions.

4.4. Preparation of stretchable Ag NWs/LIG electrode

The Ag NWs electrode was obtained by repeatedly spraying Ag NWs solution on a PDMS-Ecoflex film (2 ×2 cm^2) 5–8 times, with each spraying followed by drying at 60 °C for 2 min. The LIG was obtained by laser scribing of the PI film using a computer-controlled commercial CO_2 laser (Universal Laser, 10.6 μm, maximum power of 30 W). First, the PI film was fixed on the glass substrate using hydrosol for reduced deformation from the laser processing. Next, the CO_2 laser (power of 23%, scanning speed of 28%, image density of 500 PPI) was utilized to create the LIG on PI in one step, followed by applying the mixed silicon rubber solution to the top surface. Placing the sample in a vacuum drying oven for 30 min allowed the solution to penetrate into the porous structure of the LIG and removed excess air, which was then dried at 80 °C for 2 h for curing. Immersing the sample in clean water for 24 h removed the glass substrate. Carefully peeled off the PI film successfully transferred the LIG to the stretchable silicon rubber substrate. After pre-stretching the silicon rubber film with LIG to a given tensile strain (ε_{pre} = 0%, 10%, 20%, 30%), spraying Ag NWs solution with a spray gun and releasing the pre-strain, followed by baking at 60 °C for 5 min, generated the stretchy Ag NWs/LIG electrode on the PDMS-Ecoflex film.

4.5. Fabrication of MXene/PDMS-Ecoflex composite film

2 g of the PDMS solution at 10:1 w/w ratio was spin-coated on a 10 × 10 cm^2 glass plate at 250 rpm for 60 s. Next, 2 g of the mixed PDMS-Ecoflex solution prepared as described above was spin-coated at 250 rpm for 60 s. After adding 0.5 ml MXene solution (5 mg/ml) to another 2 g of the mixed PDMS-Ecoflex solution with magnetical stirring at 1300 rpm for 30 min, the obtained solution was then spin coated at 250 rpm for 60 s. Baking the sample at 90 °C for 1 h obtained the composite film.

4.6. Treatment of fabric samples

The fabric samples cut to a given size were first placed in a bottle containing anhydrous ethanol solution with ultrasonic treatment for 15 min. Removing the fabric samples from the bottle and placing them in a 60 °C oven for 20 min removed excessive ethanol. After drying, the samples were attached to PET with double-sided adhesive tape.

4.7. Characterization and Measurements

Tensile loading on the stretchable LIG-TENG was applied by a general material testing machine (JSV-H1000 in Japan). Scanning electron microscope (SEM) images were collected by a field emission scanning electron microscope (JEOL, JSM 7100 F). The Raman spectra of the LIG/PDMS-Ecoflex were obtained by LabRAM HR Evolution. XRD patterns of MXene and MAX were obtained by a D8 Discover X-ray diffractometer. With an exciter system (Donghua Testing Technology Co., Ltd., China) to simulate vibration, the electrical performance (i.e., open-circuit voltage, short circuit current, and transferred charge) of the LIG-TENG was measured using an oscilloscope (MDO 5104B, Tektronix, USA) with a probe of 10 MΩ, an electrochemical workstation (Vertex.C.EIS, Ivium Technologies BV, Netherlands), and an electrometer (Keithley 6514, USA). Electrometer 6514 was also used in the application demonstrations, including human behavior sensing, wind speed monitoring, home anti-theft, water droplet energy harvesting, and early warning of

water leakage.

CRediT authorship contribution statement

Li. Yang: Contributed to the conception of the study, Wrote the manuscript. **Chaosai Liu**: Led the experiments of triboelectric nanogenerators and collected the overall data, Wrote draft of manuscript. **Huanyu Cheng**: Contributed to the conception of the study, Wrote the manuscript. **Wenjing Yuan, Chuizhou Meng, Ankan Dutta**: Contributed to the theoretical analysis of the study. **Xue Chen, Langang Guo, Guangyu Niu**: Performed the data analysis and co-wrote the paper. All authors provided the feedback on the manuscript.

Declaration of Competing Interest

The authors declare that they have no known competing financial interests or personal relationships that could have appeared to influence the work reported in this paper.

Data availability

The authors are unable or have chosen not to specify which data has been used.

Acknowledgments

This work was supported by the National Natural Science Foundation of China (51705126, 61871173), and the Key Research and Development Project of Hebei Province (20271701D, 22371703D). H.C. acknowledges the support provided by NIH (Award Nos. R21EB030140, U01DA056242, and R61HL154215), NSF (Grant No. ECCS-1933072), and Penn State University.

Appendix A. Supporting information

Supplementary data associated with this article can be found in the online version at doi:10.1016/j.nanoen.2022.107807.

References

[1] C. Zhong, B. Liu, J. Ding, X. Liu, Y. Zhong, Y. Li, C. Sun, X. Han, Y. Deng, N. Zhao, W. Hu, Decoupling electrolytes towards stable and high-energy rechargeable aqueous zinc-manganese dioxide batteries, Nat. Energy 5 (2020) 440–449, https://doi.org/10.1038/s41560-020-0584-y.
[2] Y.X. Yao, X.Q. Zhang, B.Q. Li, C. Yan, P.Y. Chen, J.Q. Huang, Q. Zhang, A compact inorganic layer for robust anode protection in lithium-sulfur batteries, InfoMat 2 (2020) 379–388, https://doi.org/10.1002/inf2.12046.
[3] F. Wang, Z. Liu, C. Yang, H. Zhong, G. Nam, P. Zhang, R. Dong, Y. Wu, J. Cho, J. Zhang, X. Feng, Fully conjugated phthalocyanine copper metal-organic frameworks for sodium-iodine batteries with long-time-cycling durability, Adv. Mater. 32 (2020), 1905361, https://doi.org/10.1002/adma.201905361.
[4] Q. Zhang, Y. Ma, Y. Lu, L. Li, F. Wan, K. Zhang, J. Chen, Modulating electrolyte structure for ultralow temperature aqueous zinc batteries, Nat. Commun. 11 (2020) 4463, https://doi.org/10.1038/s41467-020-18284-0.
[5] C. Yan, H. Yuan, H.S. Park, J.Q. Huang, Perspective on the critical role of interface for advanced batteries, J. Energy Chem. 47 (2020) 217–220, https://doi.org/10.1016/j.jechem.2019.09.034.
[6] L. Jin, X. Xiao, W. Deng, A. Nashalian, D. He, V. Raveendran, C. Yan, H. Su, X. Chu, T. Yang, W. Li, W. Yang, J. Chen, Manipulating relative permittivity for high-performance wearable triboelectric nanogenerators, Nano Lett. 20 (2020) 6404–6411, https://doi.org/10.1021/acs.nanolett.0c01987.
[7] Z. Zhao, Q. Huang, C. Yan, Y. Liu, X. Zeng, X. Wei, Y. Hu, Z. Zheng, Machine-washable and breathable pressure sensors based on triboelectric nanogenerators enabled by textile technologies, Nano Energy 70 (2020), 104528, https://doi.org/10.1016/j.nanoen.2020.104528.
[8] F. Wen, Z. Sun, T. He, Q. Shi, M. Zhu, Z. Zhang, L. Li, T. Zhang, C. Lee, Machine learning glove using self-powered conductive superhydrophobic triboelectric textile for gesture recognition in VR/AR applications, Adv. Sci. 7 (2020), 2000261, https://doi.org/10.1002/advs.202000261.
[9] B. Dudem, S.A. Graham, R.D.I.G. Dharmasena, S.R.P. Silva, J.S. Yu, Natural silk-composite enabled versatile robust triboelectric nanogenerators for smart applications, Nano Energy 83 (2021), 105819, https://doi.org/10.1016/j.nanoen.2021.105819.
[10] X. Pu, H. Guo, Q. Tang, J. Chen, L. Feng, G. Liu, X. Wang, Y. Xi, C. Hu, Z.L. Wang, Rotation sensing and gesture control of a robot joint via triboelectric quantization sensor, Nano Energy 54 (2018) 453–460, https://doi.org/10.1016/j.nanoen.2018.10.044.
[11] J. Chen, X. Pu, H. Guo, Q. Tang, L. Feng, X. Wang, C. Hu, A self-powered 2D barcode recognition system based on sliding mode triboelectric nanogenerator for personal identification, Nano Energy 43 (2018) 253–258, https://doi.org/10.1016/j.nanoen.2017.11.028.
[12] S.Y. Kuang, G. Zhu, Z.L. Wang, Triboelectrification-enabled self-powered data storage, Adv. Sci. 5 (2018), 1700658, https://doi.org/10.1002/advs.201700658.
[13] H. Qin, G. Cheng, Y. Zi, G. Gu, B. Zhang, W. Shang, F. Yang, J. Yang, Z. Du, Z. L. Wang, High energy storage efficiency triboelectric nanogenerators with unidirectional switches and passive power management circuits, Adv. Funct. Mater. 28 (2018), 1805216, https://doi.org/10.1002/adfm.201805216.
[14] K. Zhou, Y. Zhao, X. Sun, Z. Yuan, G. Zheng, K. Dai, L. Mi, C. Pan, C. Liu, C. Shen, Ultra-stretchable triboelectric nanogenerator as high-sensitive and self-powered electronic skins for energy harvesting and tactile sensing, Nano Energy 70 (2020), 104546, https://doi.org/10.1016/j.nanoen.2020.104546.
[15] C. Yan, Y. Gao, S. Zhao, S. Zhang, Y. Zhou, W. Deng, Z. Li, G. Jiang, L. Jin, G. Tian, T. Yang, X. Chu, D. Xiong, Z. Wang, Y. Li, W. Yang, J. Chen, A linear-to-rotary hybrid nanogenerator for high-performance wearable biomechanical energy harvesting, Nano Energy 67 (2020), 104235, https://doi.org/10.1016/j.nanoen.2019.104235.
[16] C. Chen, L. Chen, Z. Wu, H. Guo, W. Yu, Z. Du, Z.L. Wang, 3D double-faced interlock fabric triboelectric nanogenerator for bio-motion energy harvesting and as self-powered stretching and 3D tactile sensors, Mater. Today 32 (2020) 84–93, https://doi.org/10.1016/j.mattod.2019.10.025.
[17] Q. Shi, C. Lee, Self-powered bio-inspired spider-net-coding interface using single-electrode triboelectric nanogenerator, Adv. Sci. 6 (2019), 1900617, https://doi.org/10.1002/advs.201900617.
[18] Y. Song, J. Min, Y. Yu, H. Wang, Y. Yang, H. Zhang, W. Gao, Wireless battery-free wearable sweat sensor powered by human motion, Sci. Adv. 6 (2020) eaay9842, https://doi.org/10.1126/sciadv.aay9842.
[19] W. Paosangthong, M. Wagih, R. Torah, S. Beeby, Textile-based triboelectric nanogenerator with alternating positive and negative freestanding grating structure, Nano Energy 66 (2019), 104148, https://doi.org/10.1016/j.nanoen.2019.104148.
[20] Z. Zhang, Y. Bai, L. Xu, M. Zhao, M. Shi, Z.L. Wang, X. Lu, Triboelectric nanogenerators with simultaneous outputs in both single-electrode mode and freestanding-triboelectric-layer mode, Nano Energy 66 (2019), 104169, https://doi.org/10.1016/j.nanoen.2019.104169.
[21] W. Paosangthong, M. Wagih, R. Torah, S. Beeby, Textile-based triboelectric nanogenerator with alternating positive and negative freestanding woven structure for harvesting sliding energy in all directions, Nano Energy 92 (2022), 106739, https://doi.org/10.1016/j.nanoen.2021.106739.
[22] Y. Liu, J. Ping, Y. Ying, Recent progress in 2D-nanomaterial-based triboelectric nanogenerators, Adv. Funct. Mater. 31 (2021), 2009994, https://doi.org/10.1002/adfm.202009994.
[23] H. Li, Y. Sun, Y. Su, R. Li, H. Jiang, Y. Xie, X. Ding, X. Wu, Y. Tang, Multi-scale metal mesh based triboelectric nanogenerator for mechanical energy harvesting and respiratory monitoring, Nano Energy 89 (2021), 106423, https://doi.org/10.1016/j.nanoen.2021.106423.
[24] L. Gu, L. German, T. Li, J. Li, Y. Shao, Y. Long, J. Wang, X. Wang, Energy harvesting floor from commercial cellulosic materials for a self-powered wireless transmission sensor system, ACS Appl. Mater. Interfaces 13 (2021) 5133–5141, https://doi.org/10.1021/acsami.0c20703.
[25] J. Yu, X. Hou, J. He, M. Cui, C. Wang, W. Geng, J. Mu, B. Han, X. Chou, Ultra-flexible and high-sensitive triboelectric nanogenerator as electronic skin for self-powered human physiological signal monitoring, Nano Energy 69 (2020), 104437.
[26] Z. Zheng, D. Yu, Y. Guo, Dielectric modulated glass fiber fabric-based single electrode triboelectric nanogenerator for efficient biomechanical energy harvesting, Adv. Funct. Mater. 31 (2021), 2102431, https://doi.org/10.1002/adfm.202102431.
[27] C. Jiang, C. Wu, X. Li, Y. Yao, L. Lan, F. Zhao, Z. Ye, Y. Ying, J. Ping, All-electrospun flexible triboelectric nanogenerator based on metallic MXene nanosheets, Nano Energy 59 (2019) 268–276, https://doi.org/10.1016/j.nanoen.2019.02.052.
[28] X. Li, C. Jiang, F. Zhao, L. Lan, Y. Yao, Y. Yu, J. Ping, Y. Ying, Fully stretchable triboelectric nanogenerator for energy harvesting and self-powered sensing, Nano Energy 61 (2019) 78–85, https://doi.org/10.1016/j.nanoen.2019.04.025.
[29] J. Qian, J. He, S. Qian, J. Zhang, X. Niu, X. Fan, C. Wang, X. Hou, J. Mu, W. Geng, X. Chou, A nonmetallic stretchable nylon-modified high performance triboelectric nanogenerator for energy harvesting, Adv. Funct. Mater. 30 (2020), 1907414, https://doi.org/10.1002/adfm.201907414.
[30] Y. Lee, J. Kim, B. Jang, S. Kim, B.K. Sharma, J.H. Kim, J.H. Ahn, Graphene-based stretchable/wearable self-powered touch sensor, Nano Energy 62 (2019) 259–267, https://doi.org/10.1016/j.nanoen.2019.05.039.
[31] D.W. Shin, M.D. Barnes, K. Walsh, D. Dimov, P. Tian, A.I.S. Neves, C.D. Wright, S. M. Yu, J.B. Yoo, S. Russo, M.F. Craciun, A new facile route to flexible and semi-transparent electrodes based on water exfoliated graphene and their single-electrode triboelectric nanogenerator, Adv. Mater. 30 (2018), 1802953, https://doi.org/10.1002/adma.201802953.
[32] H. Chu, H. Jang, Y. Lee, Y. Chae, J.H. Ahn, Conformal, graphene-based triboelectric nanogenerator for self-powered wearable electronics, Nano Energy 27 (2016) 298–305, https://doi.org/10.1016/j.nanoen.2016.07.009.

[33] S. Chun, W. Son, G. Lee, S.H. Kim, J.W. Park, S.J. Kim, C. Pang, C. Choi, Single-layer graphene-based transparent and flexible multifunctional electronics for self-charging power and touch-sensing systems (http:/doi.org/), ACS Appl. Mater. Interfaces 11 (2019) 9301–9308, https://doi.org/10.1021/acsami.8b20143.
[34] L. Yang, H. Ji, C. Meng, Y. Li, G. Zheng, X. Chen, G. Niu, J. Yan, Y. Xue, S. Guo, H. Cheng, Intrinsically breathable and flexible NO_2 gas sensors produced by laser direct writing of self-assembled block copolymers, ACS Appl. Mater. Interfaces 14 (2022) 17818–17825, https://doi.org/10.1021/acsami.2c02061.
[35] X. Chen, R. Li, G. Niu, M. Xin, G. Xu, H. Cheng, L. Yang, Porous graphene foam composite-based dual-mode sensors for underwater temperature and subtle motion detection, Chem. Eng. J. 444 (2022), 136631, https://doi.org/10.1016/j.cej.2022.136631.
[36] J. He, R. Zhou, Y. Zhang, W. Gao, T. Chen, W. Mai, C. Pan, Strain-insensitive self-powered tactile sensor arrays based on intrinsically stretchable and patternable ultrathin conformal wrinkled graphene-elastomer composite, Adv. Funct. Mater. 32 (2022), 2107281, https://doi.org/10.1002/adfm.202107281.
[37] M.G. Stanford, J.T. Li, Y. Chyan, Z. Wang, W. Wang, J.M. Tour, Laser-induced graphene triboelectric nanogenerators, ACS Nano 13 (2019) 7166–7174, https://doi.org/10.1021/acsnano.9b02596.
[38] C. Jiang, X. Li, Y. Yao, L. Lan, Y. Shao, F. Zhao, Y. Ying, J. Ping, A multifunctional and highly flexible triboelectric nanogenerator based on MXene-enabled porous film integrated with laser-induced graphene electrode, Nano Energy 66 (2019), 104121, https://doi.org/10.1016/j.nanoen.2019.104121.
[39] X. Li, C. Jiang, F. Zhao, Y. Shao, Y. Ying, J. Ping, A self-charging device with bionic self-cleaning interface for energy harvesting, Nano Energy 73 (2020), 104738, https://doi.org/10.1016/j.nanoen.2020.104738.
[40] Z. Yan, L. Wang, Y. Xia, R. Qiu, W. Liu, M. Wu, Y. Zhu, S. Zhu, C. Jia, M. Zhu, R. Cao, Z. Li, X. Wang, Flexible high-resolution triboelectric sensor array based on patterned laser-induced graphene for self-powered real-time tactile sensing, Adv. Funct. Mater. 31 (2021), 2100709, https://doi.org/10.1002/adfm.202100709.
[41] P. Zhao, G. Bhattacharya, S.J. Fishlock, J.G.M. Guy, A. Kumar, C. Tsonos, Z. Yu, S. Raj, J.A. McLaughlin, J. Luo, N. Soin, Replacing the metal electrodes in triboelectric nanogenerators: High-performance laser-induced graphene electrodes, Nano Energy 75 (2020), 104958, https://doi.org/10.1016/j.nanoen.2020.104958.
[42] H. Wang, Z. Zhao, P. Liu, X. Guo, A soft and stretchable electronics using laser-induced graphene on polyimide/PDMS composite substrate, npj Flex. Electron. 6 (2022) 26, https://doi.org/10.1038/s41528-022-00161-z.
[43] S. Chen, K. Jiang, Z. Lou, D. Chen, G. Shen, Recent developments in graphene-based tactile sensors and e-skins, Adv. Mater. Technol. 3 (2018), 1700248, https://doi.org/10.1002/admt.201700248.
[44] F. Shahzad, A. Iqbal, H. Kim, C.M. Koo, 2D transition metal carbides (MXenes): applications as an electrically conducting material, Adv. Mater. 32 (2020), 2002159, https://doi.org/10.1002/adma.202002159.
[45] Y. Dong, S.S.K. Mallineni, K. Maleski, H. Behlow, V.N. Mochalin, A.M. Rao, Y. Gogotsi, R. Podila, Metallic MXenes: A new family of materials for flexible triboelectric nanogenerators, Nano Energy 44 (2018) 103–110, https://doi.org/10.1016/j.nanoen.2017.11.044.
[46] R. Ye, D.K. James, J.M. Tour, Laser-Induced Graphene, Acc. Chem. Res 51 (2018) 1609–1620, https://doi.org/10.1021/acs.accounts.8b00084.
[47] J. Vaicekauskaite, P. Mazurek, S. Vudayagiri, A.L. Skov, A. Skov, Mapping the mechanical and electrical properties of commercial silicone elastomer formulations for stretchable transducers, J. Mater. Chem. C. 8 (2020) 1273–1279, https://doi.org/10.1039/C9TC05072H.
[48] Y. Tang, Y. Xu, J. Yang, Y. Song, F. Yin, W. Yuan, Stretchable and wearable conductometric VOC sensors based on microstructured MXene/polyurethane core-sheath fibers, Sens. Actuators B Chem. 346 (2021), 130500, https://doi.org/10.1016/j.snb.2021.130500.
[49] L. Yang, H. Wang, W. Yuan, Y. Li, P. Gao, N. Tiwari, X. Chen, Z. Wang, G. Niu, H. Cheng, Wearable pressure sensors based on MXene/tissue papers for wireless human health monitoring, ACS Appl. Mater. Interfaces 13 (2021) 60531–60543, https://doi.org/10.1021/acsami.1c22001.
[50] A.C. Ferrari, J.C. Meyer, V. Scardaci, C. Casiraghi, M. Lazzeri, F. Mauri, S. Piscanec, D. Jiang, K.S. Novoselov, S. Roth, A.K. Geim, Raman spectrum of graphene and graphene layers, Phys. Rev. Lett. 97 (2006), 187401, https://doi.org/10.1103/PhysRevLett.97.187401.
[51] X. Xuan, J.Y. Kim, X. Hui, P.S. Das, H.S. Yoon, J.Y. Park, A highly stretchable and conductive 3D porous graphene metal nanocomposite based electrochemical-physiological hybrid biosensor, Biosens. Bioelectron. 120 (2018) 160–167, https://doi.org/10.1016/j.bios.2018.07.071.
[52] R. Zhang, H. Olin, Material choices for triboelectric nanogenerators: A critical review, EcoMat 2 (2020), e12062, https://doi.org/10.1002/eom2.12062.
[53] S. Zhang, J. Zhu, Y. Zhang, Z. Chen, C. Song, J. Li, N. Yi, D. Qiu, K. Guo, C. Zhang, T. Pan, Y. Lin, H. Zhou, H. Long, H. Yang, H. Cheng, Standalone stretchable RF systems based on asymmetric 3D microstrip antennas with on-body wireless communication and energy harvesting, Nano Energy 96 (2022), 107069, https://doi.org/10.1016/j.nanoen.2022.107069.
[54] J. An, P. Chen, C. Li, F. Li, T. Jiang, Z.L. Wang, Methods for correctly characterizing the output performance of nanogenerators, Nano Energy 93 (2022), 106884, https://doi.org/10.1016/j.nanoen.2021.106884.
[55] T. Bhatta, P. Maharjan, H. Cho, C. Park, S.H. Yoon, S. Sharma, M. Salauddin, M. T. Rahman, S.M.S. Rana, J.Y. Park, High-performance triboelectric nanogenerator based on MXene functionalized polyvinylidene fluoride composite nanofibers, Nano Energy 81 (2021), 105670, https://doi.org/10.1016/j.nanoen.2020.105670.
[56] C. Zhang, H. Chen, X. Ding, F. Lorestani, C. Huang, B. Zhang, B. Zheng, J. Wang, H. Cheng, Y. Xu, Human motion-driven self-powered stretchable sensing platform based on laser-induced graphene foams, Appl. Phys. Rev. 9 (2022), 011413, https://doi.org/10.1063/5.0077667.
[57] D.A. Jones, O.M. Rutherford, Human muscle strength training: the effects of three different regimens and the nature of the resultant changes, J. Physiol. 391 (1987) 1–11, https://doi.org/10.1113/jphysiol.1987.sp016721.
[58] Y. Jie, X. Jia, J. Zou, Y. Chen, N. Wang, Z.L. Wang, X. Cao, Natural leaf made triboelectric nanogenerator for harvesting environmental mechanical energy, Adv. Energy Mater. 8 (2018), 1703133, https://doi.org/10.1002/aenm.201703133.
[59] Z.H. Lin, G. Cheng, S. Lee, K.C. Pradel, Z.L. Wang, Harvesting water drop energy by a sequential contact-electrification and electrostatic-induction process, Adv. Mater. 26 (2014) 4690–4696, https://doi.org/10.1002/adma.201400373.
[60] L. Zheng, Z.H. Lin, G. Cheng, W. Wu, X. Wen, S. Lee, Z.L. Wang, Silicon-based hybrid cell for harvesting solar energy and raindrop electrostatic energy, Nano Energy 9 (2014) 291–300, https://doi.org/10.1016/j.nanoen.2014.07.024.
[61] S. Nie, Q. Fu, X. Lin, C. Zhang, Y. Lu, S. Wang, Enhanced performance of a cellulose nanofibrils-based triboelectric nanogenerator by tuning the surface polarizability and hydrophobicity, Chem. Eng. J. 404 (2021), 126512, https://doi.org/10.1016/j.cej.2020.126512.
[62] S.M.S. Rana, M.T. Rahman, M. Salauddin, S. Sharma, P. Maharjan, T. Bhatta, H. Cho, C. Park, J.Y. Park, Electrospun PVDF-TrFE/MXene Nanofiber Mat-Based Triboelectric Nanogenerator for Smart Home Appliances, ACS Appl. Mater. Inter. 13 (2021) 4955–4967, https://doi.org/10.1021/acsami.0c17512.
[63] Y. Liu, W. Liu, Z. Wang, W. He, Q. Tang, Y. Xi, X. Wang, H. Guo, C. Hu, Quantifying contact status and the air-breakdown model of charge-excitation triboelectric nanogenerators to maximize charge density, Nat. Commun. 11 (2020) 1599, https://doi.org/10.1038/s41467-020-15368-9.
[64] X. Xia, J. Fu, Y. Zi, A universal standardized method for output capability assessment of nanogenerators, Nat. Commun. 10 (2019) 4428, https://doi.org/10.1038/s41467-019-12465-2.
[65] K.H. Lee, Y.Z. Zhang, Q. Jiang, H. Kim, A.A. Alkenawi, H.N. Alshareef, Ultrasound-Driven Two-Dimensional $Ti_3C_2T_x$ MXene Hydrogel Generator, ACS Nano 14 (2020) 3199–3207, https://doi.org/10.1021/acsnano.9b08462.
[66] W.T. Cao, H. Ouyang, W. Xin, S. Chao, C. Ma, Z. Li, F. Chen, M.G. Ma, A stretchable highoutput triboelectric nanogenerator improved by MXene liquid electrode with high electronegativity, Adv. Funct. Mater. 30 (2020), 2004181, https://doi.org/10.1002/adfm.202004181.
[67] X. Luo, L. Zhu, Y.C. Wang, J. Li, J. Nie, Z.L. Wang, A flexible multifunctional triboelectric nanogenerator based on MXene/PVA hydrogel, Adv. Funct. Mater. 31 (2021), 2104928, https://doi.org/10.1002/adfm.202104928.
[68] Y. Gao, G. Liu, T. Bu, Y. Liu, Y. Qi, Y. Xie, S. Xu, W. Deng, W. Yang, C. Zhang, MXene based mechanically and electrically enhanced film for triboelectric nanogenerator, Nano Res 14 (2021) 4833–4840, https://doi.org/10.1007/s12274-021-3437-5.

Li Yang is an associate professor of the School of Health Sciences and Biomedical Engineering at Hebei University of Technology. She received her Ph.D. degree in Mechanical Engineering from Hebei University of Technology in 2015. During 2018-2019, she worked as a visiting scholar in Pennsylvania State University in the USA. Her current research interests include flexible electronics, wearable intelligent sensing system, carbon-based nanomaterials and their applications in healthcare devices, disease diagnosis, biomedical sensors.

Chaosai Liu is a M.S. candidate under Associate Professor Li Yang at the Department of Health Sciences and Biomedical Engineering in Hebei University of Technology, Tianjin, China. His research interests include laser-induced graphene flexible triboelectric nanogenerator.

Wenjing Yuan obtained her Ph.D. degree (2016) from Tsinghua University. At present, she is a Research Associate of Tianjin Key Laboratory of Materials Laminating Fabrication and Interface Control Technology, College of Material Science & Engineering, Hebei University of Technology. Her current research is focused on 2D nanomaterials-based gas sensors and wearable intelligent strain sensors.

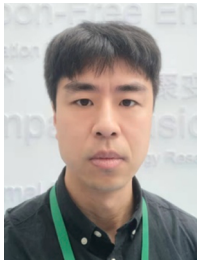

Chuizhou Meng is a professor of the School of Mechanical Engineering at Hebei University of Technology. He received his Ph.D. degree in Physics from Tsinghua University in 2011. Before joining Hebei University of Technology, he did post-doctoral research in Biomedical Engineering at Purdue University and worked as a Senior Engineer at IBM Semiconductor R&D Center in the US. His current research interests include carbon-based nanomaterials and polymeric elastomers and their applications in energy devices, biomedical sensors, wearable electronics and healthcare robot.

Ankan Dutta is a Ph.D. student under the supervision of Professor Huanyu Cheng at The Pennsylvania State University, University Park. He received his undergraduate degree from Jadavpur University in Mechanical Engineering. He had been awarded SERB Fellowships in Jadavpur University and the Indian Association for the Cultivation of Science. He has also served as a Reviewer for IEEE SMC 2022. His current research interests include soft robotics and biomedical devices such as flexible ultrasound arrays.

Xue Chen is a Ph.D. candidate under Prof. Guizhi Xu and Associate Professor Li Yang at the Department of Electrical Engineering in Hebei University of Technology, Tianjin, China. Her research interests focus on laser-induced graphene flexible wearable electronics.

Langang Guo is a M.S. candidate under Associate Professor Li Yang at the Department of Health Sciences and Biomedical Engineering in Hebei University of Technology, Tianjin, China. His research interests include liquid metal flexible triboelectric nanogenerator.

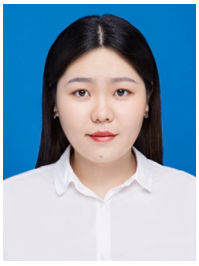

Guangyu Niu is a M.S. candidate under Associate Professor Li Yang at the Department of Health Sciences and Biomedical Engineering in Hebei University of Technology, Tianjin, China. Her research interests include paper-based flexible humidity sensors.

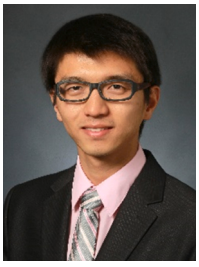

Prof. Huanyu Cheng earned a Ph.D. degree from Northwestern University in 2015 and a Bachelor's degree from Tsinghua University in 2010. He is the James L. Henderson, Jr. Memorial Associate Professor of Engineering Science and Mechanics at Penn State University. Dr. Cheng has worked on standalone stretchable sensing systems for biomedicine with over 120 peer-reviewed publications, and his work has been recognized through the reception of numerous awards. He also serves as an associate editor for IEEE Internet of Things Journal, Computers in Biology and Medicine, and reviewer for over 210 international journals.